16A.7 EVOLUTION OF BOUNDARY LAYER WIND AND MOISTURE FIELDS ALONG A FRONT DURING IHOP

John Stonitsch* and Paul Markowski

Department of Meteorology, Pennsylvania State University, University Park, PA

1. Introduction

One of the principal goals of the International H_2O Project (IHOP) was to further our understanding of spatial and temporal water vapor variability and how this variability affects convection initiation (CI). On 3 June 2002 a wealth of mobile observing systems were deployed in the Oklahoma panhandle in hopes of observing convection initiation along a front. Convection failed to be initiated along the front, likely as a result of tremendous convective inhibition (CIN). Values as large as 400 J kg^{-1} were observed on soundings launched in the area.

Even though this case may not seem like an enticing convection initiation case—or perhaps even a good convection initiation failure case, owing to the rather obvious reason for failure (that being the very unfavorable large-scale conditions promoting the large CIN)—a possibly unprecedented dataset was obtained along the front. High-resolution radar data collected by four mobile radars afforded nearly seven continuous hours of dual-Doppler wind syntheses from 1600–2300 UTC as the front moved slowly southward as a cold front, stalled, and then retreated northward as a warm front. Furthermore, the intercept occurred in the vicinity of the National Center for Atmospheric Research (NCAR) S-band dual-Polarization Doppler radar (SPOL). Refractivity measurements from SPOL allowed the low-level moisture field to be retrieved in the vicinity of the front.

Our ongoing research includes a thorough analysis of the three-dimensional kinematic fields synthesized from the Doppler radar data, and the refractivity-derived moisture field along the front. This paper reports some of the results obtained thusfar.

2. Synoptic setting

The front was weak as it slowly moved southward as a cold front through southwestern Kansas and into the Oklahoma panhandle during the morning and early afternoon of 3 June. Air immediately ahead of the front was hot and dry with afternoon temperatures ranging from 34–37°C and dew points ranging from 7–11°C as strong southwest winds advected air from the high terrain of New Mexico toward the Oklahoma panhandle. Slightly cooler, more humid air was in place north of the front with temperatures ranging from 30–33°C and dewpoints

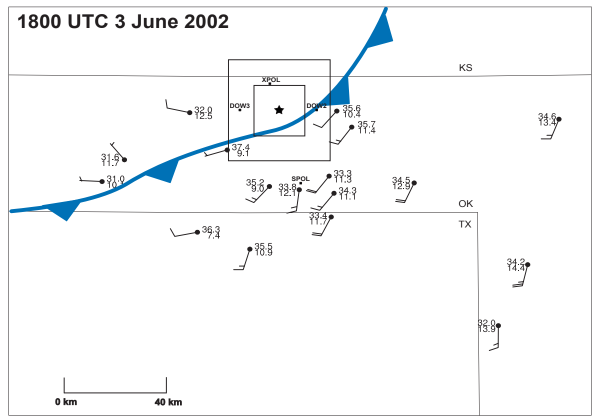

Fig. 1. Surface plot of temperature (°C), dew point (°C) and surface winds (one barb = 10 kts.) in the region surrounding the multi-Doppler analysis domain. The small box matches the area shown in Figs. 2–4 and has dimensions 20×20 km^2, while the large box spans 40×40 km^2.

ranging from 10–13°C (Fig. 1). The middle levels of the troposphere were quite warm, with 700 mb temperatures around 15°C resulting in CIN >400 J kg^{-1} on the 1800 UTC Dodge City, Kansas sounding. Visible satellite imagery showed a band of high clouds that spread northeastward from the Texas panhandle into south-central Kansas ahead of the front. This band served to keep surface temperatures slightly cooler than they otherwise would have been. Storms developed well north of the front on the high plains of western Kansas and eastern Colorado during the late afternoon and evening, but failed to form in the target domain along the front.

3. Data and analysis methods

The mobile radar data used in these analyses were collected by two Doppler on Wheels radars and the XPOL radar, which have specifications similar to those described by Wurman et al. (1997). These radars operated with a half-power beam width of 0.93° and a Nyquist velocity of 16 m s^{-1}. The SPOL radar as described by Lutz et al. (1995) has a 0.93° half-power beam width and was fixed near Balko, Oklhaoma throughout IHOP. The positions of the radars are indicated in Fig. 1.

Mobile radar data were first rotated to the correct azimuth using a combination of solar calibration (Arnott et al. 2003a) and geo-referencing using identifiable ground clutter targets such as relay towers and telephone poles. Once rotated, spurious data caused by low signal-to-noise ratio, velocity aliasing, second-trip echoes, and

Corresponding author address: John R. Stonitsch, Department of Meteorology, Pennsylvania State University, 503 Walker Building, University Park, PA 16802; *e-mail*: jrs390@psu.edu.

ground clutter were removed. Finally, an advection correction was applied that minimizes the time derivatives of the velocity components. Matejka's (2002) technique was used to obtain the appropriate advection velocity.

Edited data were objectively analyzed onto a Cartesian grid using an isotropic spherical Barnes weight function with a radius of influence of 1 km. Our choice of smoothing parameter, κ, follows the recommendation of Pauley and Wu (1990), where specification of κ depends on the coarsest data spacing (Trapp and Doswell 2000). The grid has dimensions $40 \times 40 \times 1$ km^3.

Refractivity data were collected by the SPOL radar located approximately 30 km south of the center of the multi-Doppler domain. Noise was removed and data were objectively analyzed using a Barnes scheme and κ of 0.55 km^2. Refractivity was then converted to vapor pressure via (1) (Fabry et al. 1997),

$$N = 77.6\frac{P}{T} + 3.73 \times 10^5 \frac{e}{T^2}, \qquad (1)$$

where N is refractivity, T is absolute temperature (K), P is pressure (mb), and e is water vapor pressure (mb). Surface pressure and temperature were estimated at 915 mb and 35°C in the calculations. Refractivity-derived moisture fields measured by SPOL have been found to be well-correlated with low-level moisture observations obtained from other sensors, both direct and indirect (Pettet et al. 2003).

Wind syntheses were created using the overdetermined dual-Doppler approach (Kessinger et al. 1987) and upward integration of the mass continuity equation. The temporal resolution is 90 s for the wind fields and 300 s for the specific humidity field.

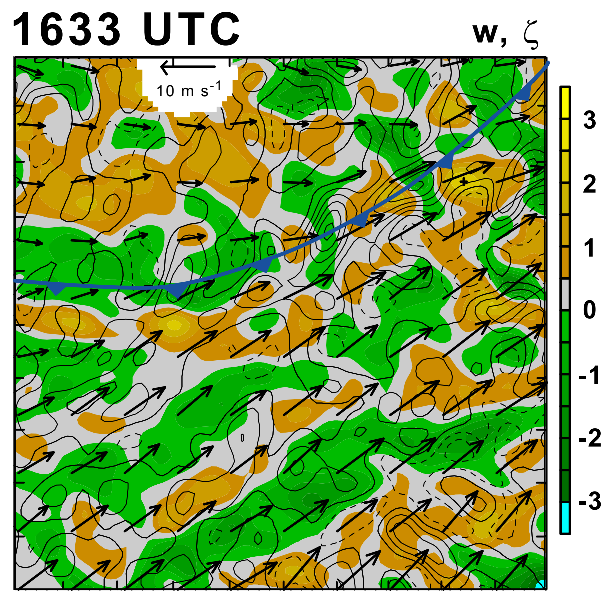

Fig. 2. Horizontal cross section of vertical vorticity (ζ; contoured at 1×10^{-3} s^{-1}) at 1 km and near-ground winds (m s^{-1}; dashed contours are negative) overlaid upon the vertical velocity (w; color shading) at 1 km at 1633 UTC. The distance between tick marks on the domain borders is 4 km.

4. Observations

At most times, the front can be easily identified in both the moisture and vorticity fields, and is generally less evident in the vertical motion (w) and convergence fields. Throughout the observation period, vorticity maxima strengthen and weaken along or just ahead of the front as they move northeastward with the flow. Vorticity maxima at the front reach values between 5×10^{-3} s^{-1} and 10×10^{-3} s^{-1} whereas values rarely exceed 5×10^{-3} s^{-1} away from it.

Strong and persistent vertical motions are not focused along the front prior to around 1700 UTC, which in some instances makes the boundary less than obvious in the w field. Vertical motions associated with boundary layer convection are nearly as strong as those associated with the front (Fig. 2). Maximum vertical velocities at 1 km are around 3 m s^{-1}.

There has been much attention given to the possible relationship between vorticity maxima and upward motions in the boundary layer both near and away from mesoscale boundaries. In some environments, updraft maxima and vertical vorticity maxima are well correlated (e.g., Kanak et al. 2000). In the 3 June 2002 case, vortices are occasionally coincident with vertical velocity maxima (Fig. 3), especially near the strengthening front.

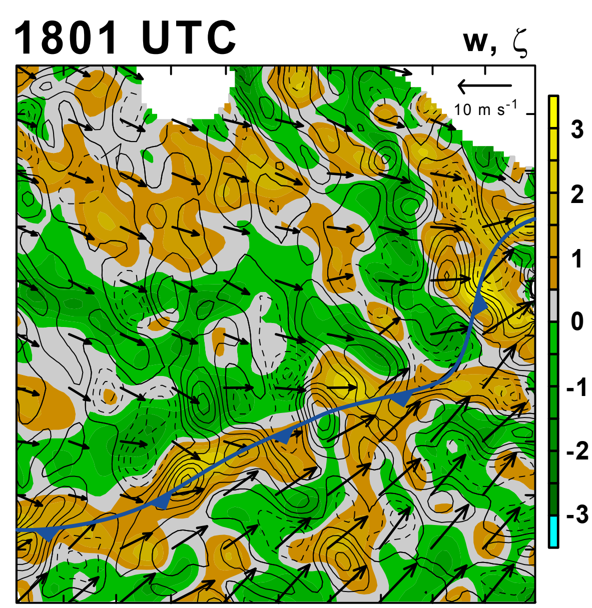

Fig. 3: As in Fig. 2, but for 1801 UTC.

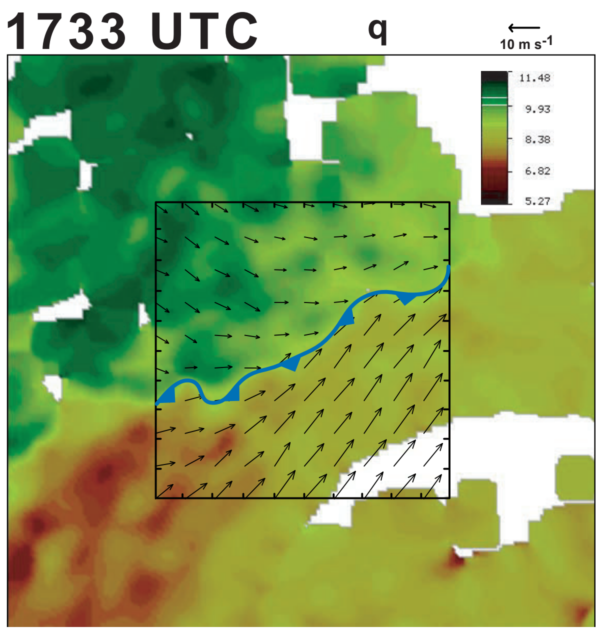

FIG. 4. Surface wind vectors and refractivity-derived specific humidity (q; color shading) at 1733 UTC. Dimensions of the interior box are 20×20 km^2, while the color moisture field spans 40×40 km^2.

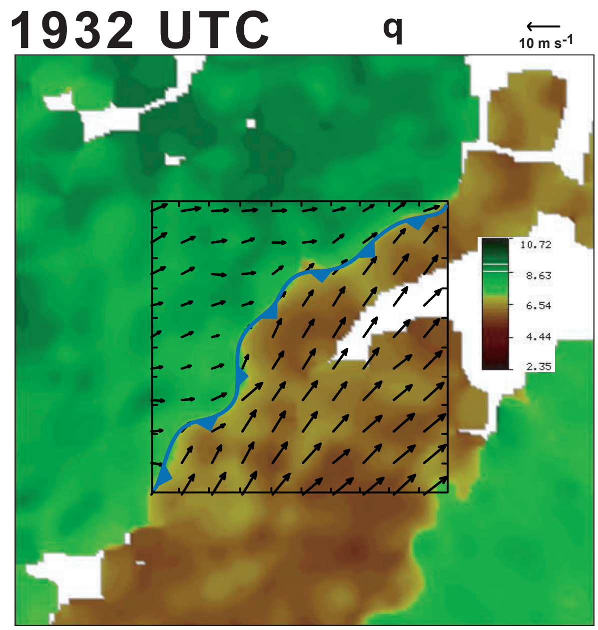

FIG. 5. As in Fig. 4, but for 1932 UTC with the grid center approximately 10 km south of its location in Figs. 1–4.

The domain-wide correlation is small on average, however, as some other IHOP investigators also have found (e.g., Arnott et al. 2003b; Hannon and Markowski 2003).

Prior to 1700 UTC, the front separates 8.0–9.0 g kg^{-1} mixing ratios to its south from 9–10.5 g kg^{-1} mixing ratios to its north. These mixing ratios correspond to surface dewpoints between 9–11°C south of the front and between 11–13°C north of the front, which are very similar to direct surface observations made during the same time period. Previous work by Weckwerth et al. (1996) has shown that small-scale moisture variability of 1.5–2.5 g kg^{-1} can occur in boundary layers containing horizontal convective rolls. Such variability is present in the surface moisture field, however it is unlikely that such variations are caused by horizontal convective rolls. Unlike the vorticity and w anomolies that move with the flow, the small-scale surface moisture anomolies remain nearly stationary, and thus would not correspond with roll signatures that are in the w field.

After 1700 UTC, the front appears to strengthen as convergence and upward motion become better focused along it (Fig. 3). During this period a surge of drier and warmer air with mixing ratios 1–2 g kg^{-1} lower arrives from the southwest (Fig. 4). Subsequently, mixing ratios south of the front range from 6.5–8.0 g kg^{-1}, with the driest air located immediately ahead of the front. At 1930 UTC a line of upward motion, many vorticity maxima and a large moisture gradient remain well-aligned with the front. Over the next hour, the southwest portion of the front bulges eastward while the northeast portion remains nearly stationary (Fig. 5). Associated with this protrusion is a strong vorticity maximum at its leading edge and corresponding bulge in the moisture field. Of note are the many wave-like structures within the boundary during this time.

5. Summary and future work

Below is a summary of major observations made in this case.

- Values of CIN in excess of 400 J kg^{-1} likely precluded deep moist convection.
- Moisture concentrations were larger north of the front, which initially moved slowly southward and then became stationary.
- The largest boundary layer vorticity maxima were located along the front.
- Vertical motions at the front often were not any stronger than those associated with boundary layer convective cells away from it. Vertical velocity magnitudes at 1 km ranged from 1–3 m s^{-1}.
- Upward motion intensified and became better defined at the front after a surge of warmer, drier air arrived from the southwest ahead of the front.

Even though this case may not be a great example of a convection initiation case, observations made in this study possibly might have implications for CI in other cases in which the large-scale environment is more favorable. One critical issue seems to be related to the superpositioning of motions induced by mesoscale, frontal dynamics and motions associated with the ubiquitous buoyant convection in the boundary layer. How are their relative contributions to the vertical motion field affected by the baroclinity observed along the front? Do the relative contributions mostly impact the magnitude of the vertical motions or the spatial patterns of the vertical motions, and what are the consequences for parcel trajectories in the vicinity of fronts? In addition, our observations indicate that refractivity-derived moisture fields are a useful tool for viewing small-scale phenomena such as the aforementioned dry surge that could easily be missed by the conventional observational network or even state mesonets. Because slight perturbations in moisture can make the difference between the initiation of deep, moist convection and scattered cumulus clouds (Crook 1996), the high spatial and temporal resolution of such moisture fields could be of great value operationally.

Future work will investigate how the front weakened and strengthened as it stalled and retreated northward. Thermodynamic retrievals will be used to assess the temperature structure near the front in order to better understand this evolution. In addition to using absolute refractivity measurements, a field of relative refractivity changes in time (also collected by SPOL) will be analyzed as it has been suggested that this is a more reliable method for analyzing small-scale moisture changes.

Acknowledgments. We are thankful for the ongoing assistance provided by Dr. Yvette Richardson, Dr. Josh Wurman, Dr. Erik Rasmussen, Dr. Fred Fabry, Ms. Nettie Arnott, Mr. Jeff Frame, Mr. Jim Marquis, and Mr. Christopher Shabbott. This work has been supported by NSF grant ATM-0130307 made to Pennsylvania State University.

REFERENCES

Arnott, N., Y. Richardson, J. Wurman, and J. Lutz, 2003: A solar calibration technique for determining radar pointing angles. Preprints, *31st Conf. on Radar Meteorology*, Seattle, Amer. Meteor. Soc, 492–494.

Arnott, N., Y. Richardson, and J. Wurman, 2003: A multi-doppler analysis of convective initiation on 10 June 2002 during IHOP 2002. Preprints, *31st Conf. on Radar Meteorology*, Seattle, Amer. Meteor. Soc, 778–781.

Crook, N. A., 1996: Sensitivity of moist convection forced by boundary layer processes to low-level thermodynamic fields. *Mon. Wea. Rev.*. **124**, 1767–1785.

Fabry, F., C. Frush, I. Zawadzki, A. Kilambi, 1997: On the extraction of near-surface index of refraction using radar phase measurements from ground targets. *J. Atmos. Oceanic Technol.*, **13**, 978–987.

Hannon, C. D., P. Markowski, 2003: A multi-Doppler radar analysis of intersecting boundaries during IHOP. Preprints, *31st Conf. on Radar Meteorology*, Seattle, Amer. Meteor. Soc, 782–785.

Kanak, K., D. K. Lilly, and J. T. Snow, 2000: The formation of vertical vortices in the convective boundary layer. *Quart. J. Royal Meteor. Soc.*, **3**, 2789–2810.

Kessinger, C. J., P. S. Ray, and C. E. Hane, 1987: The Oklahoma squall line of 19 May 1977. Part I: A multiple Doppler analysis of convective and stratiform structure. *J. Atmos. Sci.*, **44**, 2840–2864.

Lutz, J., P. Johnson, B. Lewis, E. Loew, M. Randall, and J. VanAndel, 1995: NCAR's S-POL: Portable polarimetric S-band radar. Preprints, *Ninth Symp. On Meteorological Obs. and Instrumentation*, Charlotte, Amer. Meteor. Soc, 408–410.

Matejka, T., 2002: Estimating the most steady frame of reference from Doppler radar data. *J. Atmos. Oceanic Technol.*, **19**, 1035–1048.

Pauley, P. M., X. Wu, 1990: The theoretical, discrete, and actual response of the Barnes objective analysis scheme for one and two-dimensional fields. *Mon. Wea. Rev.*. **114**, 1145–1164.

Pettet, C. R., T. M. Weckworth, F. Fabry, and J. W. Wilson, 2003: An evaluation of the radar refractivity retreival during IHOP 2002. Preprints, *31st Conf. on Radar Meteorology*, Seattle, Amer. Meteor. Soc, 753–756.

Trapp, J. R., C. Doswell, 2000: Radar data objective analysis. *J. Atmos. Oceanic Technol.*, **17**, 105–120.

Weckworth, T.M., J. W. Wilson, R. M. Wakimoto, 1996: Thermodynamic variability within the convective boundary layer due to horizontal convective rolls. *Mon. Wea. Rev.*. **124**, 769–784.

Wurman, J., J. Straka, E. Rasmussen, M. Randall, and A. Zahrai, 1997: Design and deployment of a portable, pencil-beam, pulsed, 3-cm Doppler radar. *J. Atmos. Sci.*, **14**, 1502–1512.